Photoemission study of the Na/ZnSe(100) interface

Zhonghui Chen* and D. Eich
Experimentelle Physik II, Universität Würzburg, Am Hubland, D-97074 Würzburg, Germany

G. Reuscher and A. Waag
Experimentelle Physik III, Universität Würzburg, Am Hubland, D-97074 Würzburg, Germany

R. Fink and E. Umbach
Experimentelle Physik II, Universität Würzburg, Am Hubland, D-97074 Würzburg, Germany
(Received 26 February 1999)

We report on a comprehensive study of the ZnSe(100)-$c(2\times2)$-Na interface using x-ray and UV photoemission, and x-ray-induced Auger spectroscopy. Spectra were taken after stepwise Na deposition onto a clean $c(2\times2)$-reconstructed ZnSe(100) surface at room temperature up to a saturation coverage of about 1 ML of Na and after annealing. Based on the analysis of Auger parameters and of the relative intensity evolution of various Na, Zn, and Se species, we present the following model for the ZnSe(100)-$c(2\times2)$-Na interface: below a coverage of 0.5 ML, Na is adsorbed on Zn vacancy sites; above 0.5 ML, a cation exchange reaction occurs between Na and Zn atoms; Zn atoms segregate on top of the Na overlayer forming metallic Zn. In addition, band-bending, surface dipole, valence-band and surface states will be discussed.
[S0163-1829(99)02336-X]

I. INTRODUCTION

ZnSe is one of the important II-VI semiconductors due to its application in optoelectronic devices. The metal-ZnSe interface is an important aspect for such devices. Photoemission studies of metal-ZnSe interfaces provide microscopic insight into the chemical and electronic properties of the interface.[1–3] Moreover, the deposition of alkali metals on solid surfaces is extensively employed in technological processes. For example, alkali metals adsorbed on semiconductor surfaces were shown to be efficient catalytic promoters in the oxidation and nitridation of semiconductors.[4,5] In addition, alkali metals can also be used to control band offsets at heterojunctions, as was experimentally shown for the SiO_2/Si interface doped with a Cs interlayer.[6]

Alkali-metal/ZnSe interfaces are of particular interest for several reasons. First, substitutional alkali atoms in ZnSe serve as acceptors. Up to now, it has been a puzzle that the compensated acceptor concentration of alkali-doped ZnSe can hardly exceed 10^{17} cm^{-3}.[7] The electronic and chemical information on alkali/ZnSe interfaces, as extracted from photoemission spectra, is expected to be very useful for an understanding of this puzzle. Second, the Zn-Se bond has a relatively large ionic character. The heat of formation of ZnSe (-163 kJ/mol) is nearly twice as large as that for the covalent semiconductors GaAs and InP (-88 and -88.7 kJ/mol, respectively).[8] Comparison with these materials may then provide insight into reaction pathways and interdiffusion. For example, the Au/GaAs interface is reactive, leading to some exchange of atoms,[9] while the Au/ZnSe interface remains abrupt mainly due to its different cohesive energy.[1] Third, alkali-metal overlayers have been regarded as model systems for metal-semiconductor interfaces due to their simple electronic structure and their chemically active nature. The most extensive studies on alkali adsorbates on semiconductor surfaces using photoemission have concentrated on group-IV and -III-V semiconductors, particularly Si and GaAs.[10] To our knowledge, there are no photoemission studies on alkali/ZnSe interfaces yet. Moreover, previous studies on interfaces of alkali/Si, alkali/GaAs, etc.[10] have shown that only approximately 1 ML of alkali atoms can be grown on semiconductor surfaces at room temperature. Finally, it appears feasible to identify semiconductor surface states from valence-band spectra by Na exposure.

In this paper we report on an x-ray photoemission (XPS), UV photoemission (UPS), and x-ray-induced Auger spectroscopy (XAES) study of the room-temperature evolution of the ZnSe(100)-$c(2\times2)$-Na interface. We begin with a discussion of the chemistry of Na/ZnSe interfaces at room temperature. Based on the Auger parameters and the relative intensity evolution of various Zn, Se, and Na species, we conclude that the Na/ZnSe(100)-$c(2\times2)$ interface is reactive with the appearance of a ''metallic'' Zn species at Na saturation coverage, while the Na species remain nonmetallic even at saturation coverage. The valence bands of the Na/ZnSe(100) interface exhibit a metal-like Fermi cutoff due to the formation of Zn clusters. Quantitative XPS analyses indicate that Na can be deposited on the ZnSe(100)-$c(2\times2)$ surface at room temperature up to saturation coverage ($\approx$1 ML of Na), and that the growth of Na on ZnSe(100)-$c(2\times2)$ consists of two stages which are separated by a critical Na coverage of 0.5 ML. Below 0.5 ML of sodium is probably adsorbed on Zn sites, while above 0.5 ML a reaction occurs, for which an interface model is suggested. Band bending, surface dipoles, and Fermi-level pinning will be discussed. Finally, we shall identify a peak in the ZnSe valence band as a surface state.

II. EXPERIMENTAL DETAILS

The experiments were performed on undoped ZnSe layers (approximately 1 mm thick) grown by molecular-beam epi-

taxy (MBE) on undoped *n*-type ZnSe(100) single-crystal substrates. Such substrates were also employed for the growth of ZnSe-based light-emitting diodes in order to avoid stacking faults. Structural defects as observed for MBE-grown ZnSe on GaAs substrates are believed to be the key factor which presently limits the useful lifetime of II-VI light-emitting diodes and laser diodes. Clean ZnSe(100) surfaces with $c(2\times2)$ reconstruction, as monitored by low-energy electron diffraction (LEED), were prepared by sputtering with 1-keV Ar^+ ions and subsequent annealing at 400 °C for 20 min in UHV. Photoemission experiments were performed in a modified VG ESCALAB MkII (base pressure 8×10^{-11} mbar). For XPS and XAES studies Mg $K\alpha$ and Al $K\alpha$ radiation were employed and for UPS studies He I and He II radiation were employed. All photoemission spectra were recorded at normal emission angle except where specified. All binding energies are given with respect to the Fermi energy of a sputter-cleaned Au foil in electrical contact with the ZnSe sample and the spectrometer. Throughout the experiments, possible charging artifacts were eliminated by illumination with a halogen lamp.

Na was thermally evaporated out of carefully outgased alkaline dispenser elements (SAES getters) and successively deposited onto the ZnSe(100)-$c(2\times2)$ surface at room temperature. XPS and UPS were measured in several evaporation series in order to avoid any contamination. An absolutely accurate determination of the alkali coverage appears to be difficult since a quartz microbalance cannot be used to calibrate the alkali film thickness due to the relatively low sticking coefficient of alkali atoms at room temperature. The Na coverage in this paper was determined by comparing the absolute Na 1*s* peak intensity on ZnSe(100) with that of a saturated Na monolayer on Ni(111), which is known from a detailed quantitative study[11]. 1 ML of Na in the ZnSe case corresponds to an alkali coverage, for which the whole ZnSe(100) surface is covered by Na atoms in direct contact with the substrate (adsorbate density 6.27×10^{14} atoms/cm^2). Such a calibration is accurate only within $\pm10\%$ mainly due to instabilities of x-ray source, sample position, and surface. The Zn 2*p* and Zn 3*d* core-level spectra were decomposed into bulk and surface (interface) components using a χ^2-minimization procedure. This employs a symmetric Voigt line shape after subtraction of a cubic polynomial background.[12] The Zn 2*p* components could be fitted with a Lorentzian of width 0.66 eV and a Gaussian of width 1.13 eV, including the instrumental broadening of the x-ray source and spectrometer. The Zn 3*d* components measured with UPS could be fitted with a Lorentzian of width 0.15 eV, a spin-orbit splitting of 0.31 eV,[13] and a branching ratio of 1.5.

III. RESULTS AND DISCUSSION

A. Chemistry and stoichiometry of Na/ZnSe(100) interfaces

The He II excited photoemission spectra displayed in Fig. 1 show the evolution of the Zn 3*d* shallow core level after successive Na deposition on the ZnSe(100) surface. The spectrum of the clean ZnSe(100)-$c(2\times2)$ surface shows two components, which have been extensively studied before.[1,14,15] The prominent component at 10.8 eV corresponds to contributions from bulk atoms. The shoulder on

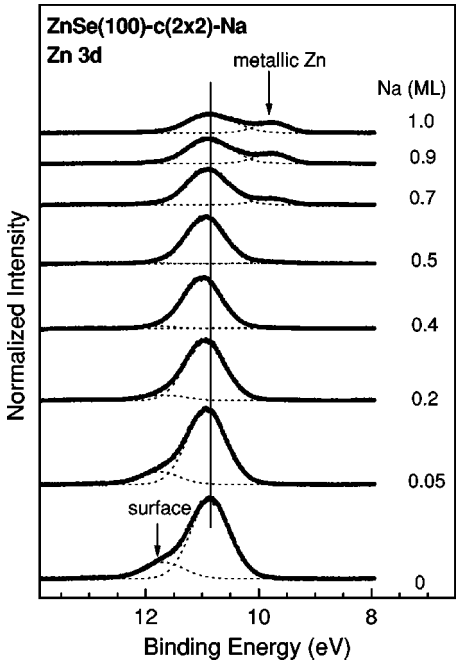

FIG. 1. He II excited photoemission spectra of the Zn 3*d* level of the ZnSe(100)-$c(2\times2)$ surface after stepwise Na deposition at room temperature. The Zn 3*d* surface-shifted component on the high-binding-energy side disappears at ~0.5-ML Na coverage. A new Zn 3*d* component on the low-binding-energy side appears instead. The dotted curves represent Voigt fits to the experimental data.

the high-binding-energy side is attributed to a surface-shifted Zn 3*d* component. The surface core-level shift is 0.84 eV, which agrees with that given in previous publications.[13,14] With increasing Na coverage, the intensity of the surface component decreases, and the Zn 3*d* bulk component shifts toward higher binding energy due to a downward band bending in the ZnSe substrate. Above a Na coverage of approximately 0.5 ML the Zn 3*d* surface component vanishes completely, while the Zn 3*d* bulk component begins to shift toward lower binding energy indicating an upward band bending. Simultaneously, the intensity of the Zn 3*d* bulk component decreases significantly due to the altered overlayer and the short mean free path of photoelectrons with a kinetic energy of ≈25 eV. Moreover, a new Zn 3*d* component appears on the low-binding-energy side above 0.5 ML of Na coverage. Its intensity increases with increasing Na coverage. Similar to Na/Si and Na/GaAs,[10] the Na coverage also shows a saturation at about 1 ML, as will be discussed later. This new Zn 3*d* component indicates the existence of a ''new'' Zn species. From its observation we conclude that the ZnSe(100)-$c(2\times2)$-Na interface at room temperature undergoes a reaction above a critical Na coverage of ≈0.5 ML. In addition, LEED measurements show the loss of the $c(2\times2)$ superstructure spots with increasing Na coverage, while the 1×1 spots become weak, directly indicating that the long-range order in the overlayer is lost.

Figure 2 shows the evolution of the Zn $2p_{3/2}$ level with Na deposition. For the clean surface a major, slightly asymmetric peak at 1022.9 eV representing the Zn bulk atoms is observed, which probably also contains a surface-shifted component on the high-binding-energy side. However, due

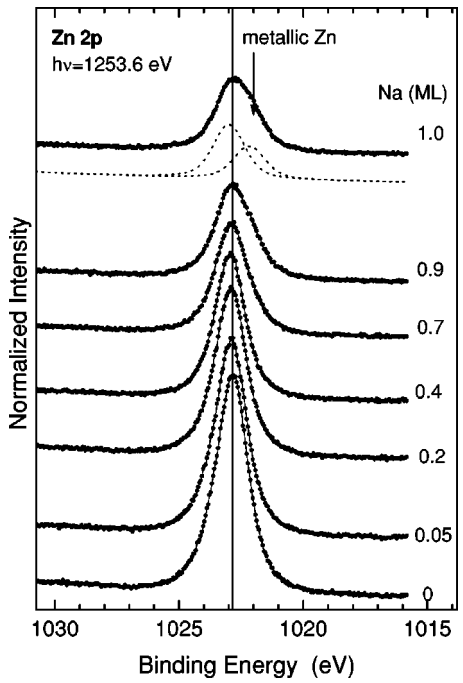

FIG. 2. Mg $K\alpha$ Zn $2p_{3/2}$ spectra of the ZnSe(100)-$c(2\times2)$ surface after stepwise Na deposition at room temperature. Near Na saturation coverage a ''metallic'' Zn $2p$ component appears on the low binding energy side.

to the poor resolution of the XPS experiment, and due to its reduced surface sensitivity, this shoulder cannot be resolved. With increasing Na coverage, the intensity of the Zn bulk component decreases because of the Na overlayer. At 1-ML Na coverage, the Zn $2p_{3/2}$ peak clearly shows another component on the low-binding-energy side. This Zn $2p$ component corresponds to the above-mentioned ''new'' Zn species. The equivalent behavior of the inner valence $(3d)$ and core $(2p_{3/2})$ levels corroborates our conclusion that the ZnSe(100)-$c(2\times2)$-Na interface is reactive.

Before further analysis, it should be noted that an unambiguous assignment of the chemical state of the ''new'' Zn species using only photoemission data appears to be impossible for the following reasons. Semiconductors have a band gap of the order of 1 eV, while chemical shifts of adsorbates are of the same order in many cases. Thus, for the same chemical state on different semiconductor surfaces, different band bending due to different doping or surface defects could lead to significant core-level differences comparable to those of chemical shifts. This means that in some cases it is difficult to distinguish between chemical shift and band bending. Thus, for the same chemical states, different core-level binding energies were observed and reported. Especially in the case of ZnSe, the Zn $2p_{3/2}$ energy range of known Zn compounds is 2.5 eV wide,[16] just smaller than the ZnSe band gap of 2.7 eV. In addition, surface photovoltage[17] and charging effects further complicate the assignment of chemical species on semiconductor surfaces. However, the concept of the so-called Auger parameter, which is independent of band bending and charging, can avoid the above-mentioned problem of chemical state assignment. Therefore we simultaneously took Auger and XPS spectra.

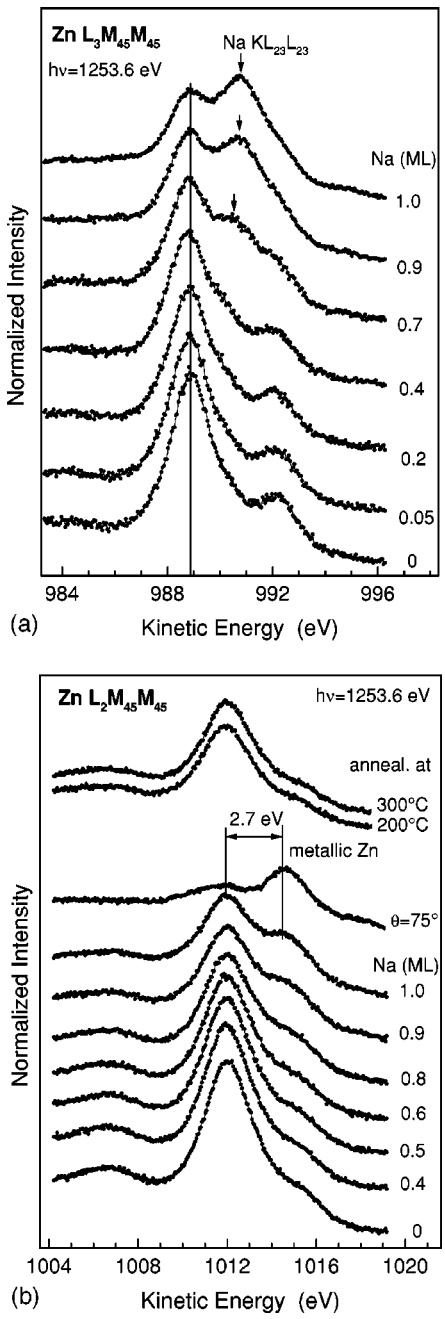

FIG. 3. (a) Zn $L_3M_{45}M_{45}$, and Na $KL_{23}L_{23}$ and (b) Zn $L_2M_{45}M_{45}$ Auger spectra of the ZnSe(100)-$c(2\times2)$ surface after stepwise Na deposition at room temperature. Near Na saturation coverage the prominent Auger peak in (a) is attributed to a Na $KL_{23}L_{23}$ transition. In (b), a new ''metallic'' Zn $L_2M_{45}M_{45}$ component appears on the high-kinetic-energy side near a Na saturation coverage which becomes more pronounced at grazing emission angle ($\theta=75°$). The metallic component disappears upon annealing.

In the Zn $L_3M_{45}M_{45}$ Auger spectra, needed for the Auger parameter and, shown in Fig. 3(a), an Auger component indicated by arrows appears at about 990.5 eV with increasing Na coverage. It becomes dominant at 1 ML of Na and can unambiguously be attributed to a Na $KL_{23}L_{23}$ Auger transition. We also measured the evolution of the Zn $L_2M_{45}M_{45}$ Auger transition with Na deposition, as shown in Fig. 3(b). At 1-ML Na coverage, a Zn $L_2M_{45}M_{45}$ component with a

smaller intensity than the bulk component appears on the high-kinetic-energy side. This component becomes dominant when the Auger spectrum is taken at grazing emission angle (75°), yielding a higher surface sensitivity. This component with a kinetic energy shift of 2.7 eV relative to the bulk component corresponds to the ''new'' Zn species observed by XPS/UPS. The 1-ML spectrum recorded at grazing emission strongly suggests that the ''new'' Zn species is located on the surface. Obviously, in Fig. 3(a) the ''new'' Zn $L_3M_{45}M_{45}$ component is hidden under the Na $KL_{23}L_{23}$ peak.

The Auger parameter of the ''new'' Zn species, discernible in Figs. 1–3, can be calculated with the assumption that the chemical shift between the Zn bulk and the ''new'' Zn component is the same for the Zn $L_2M_{45}M_{45}$ and the Zn $L_3M_{45}M_{45}$ Auger peaks. This assumption is reasonable since both transitions involve the same shallow core levels M_{45} (Zn $3d_{3/2}$ and $3d_{5/2}$). Here we define the Zn Auger parameter as in Ref. 16:

$$\alpha(\mathrm{Zn}) = E_B(\mathrm{Zn}\ \ 2p_{3/2}) + E_K(\mathrm{Zn}\ \ L_3M_{45}M_{45}).$$

For the Zn bulk component we derive α(Zn,bulk) $=2011.7$ eV. This value is in good agreement with that for the ZnSe bulk (2011.5 eV) given in Ref. 16. Furthermore, we calculate the kinetic energy of the ''new'' Zn $L_3M_{45}M_{45}$ component using the above assumption and derive α(Zn,new species) $=2013.7$ eV. Compared with compiled Auger parameters,[16] this value is in perfect agreement with that of ''metallic'' Zn [2013.8 eV (Ref. 16)], while the Auger parameters of other Zn chemical states are below 2012.9 eV. Therefore, we must conclude that the ''new'' Zn species observed in Zn $3d$, Zn $2p_{3/2}$, and Zn $L_2M_{45}M_{45}$ spectra with 1-ML Na coverage is a metallic Zn species which no longer has ionic character as in ZnSe.

Next we analyze the chemical states of Na and Se on the ZnSe(100) surface with 1-ML Na coverage. Figures 4(a) and 4(b) show the evolution of the Na $1s$ and Na KL_1L_{23} spectra with increasing Na coverage. The Na 1s peak shifts toward lower binding energy, and its line shape becomes slightly asymmetric, as seen at 1-ML Na coverage. This may be due to the following two reasons: (1) the Na overlayer becomes more metallic at high Na coverage, resulting in a more asymmetric Doniach-Sunjic line shape; or (2) there are (at least) two Na components. A clear argument can be derived from the Auger parameter of Na at 1-ML Na coverage calculated from the corresponding peaks of Figs. 2 and 4(a):

$$\alpha(\mathrm{Na}) = E_B(\mathrm{Na}1s) + E_K(\mathrm{Na}\ \ KL_{23}L_{23}) = 2063.5\ \mathrm{eV}.$$

This is by far lower than the ''metallic'' Na Auger parameters (2064.8–2066.1 eV), and significantly higher than those of known ionic Na chemical states (maximum value 2062.8 eV).[16] Unfortunately the value of Na_2Se is absent in the data compilation. Thus it can be concluded that the Na atoms on the ZnSe(100)-$c(2\times2)$ surface at room temperature are nonmetallic (or intermediate between ''metallic'' and ''ionic''), and the asymmetric Na line shape is due to the existence of different Na components. Furthermore, the Na Auger parameters evaluated for different Na coverages are about equal within the experimental uncertainty of 0.3 eV. This implies that the different Na species on the ZnSe(100)-$c(2\times2)$ surface possess similar ionicities.

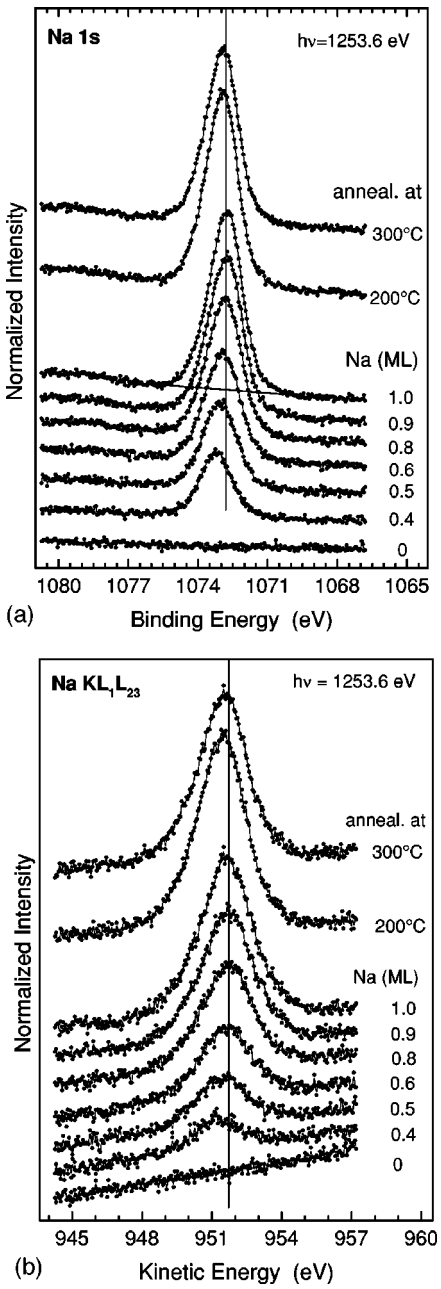

FIG. 4. (a) Na $1s$ XP spectra and (b) Na KL_1L_{23} Auger spectra of the ZnSe(100)-$c(2\times2)$ surface after stepwise Na deposition at room temperature, and after subsequent annealing for 5 min. At Na saturation coverage, the Na $1s$ line shape is asymmetric due to the existence of different Na species. Solid lines are intended as guides to the eye.

The evolution of Se $3d$ and Se $L_3M_{45}M_{45}$ peaks with increasing Na coverage is shown in Figs. 5(a) and 5(b). The Se $3d$ and Se $L_3M_{45}M_{45}$ spectra were recorded using Mg and Al $K\alpha$ irradiation, respectively. In Fig. 5(a), a satellite structure appears for the clean ZnSe(100)-$c(2\times2)$ surface on the high-binding-energy side, with an energy separation to the main line of approximately 11 eV. This satellite is attributed to a ZnSe bulk plasmon. With increasing Na coverage, the intensities of Se $3d$ and Se $L_3M_{45}M_{45}$ decrease markedly. The Se $3d$ line shape becomes wider at Na saturation coverage, as is more clearly seen in the Se $3d$ spec-

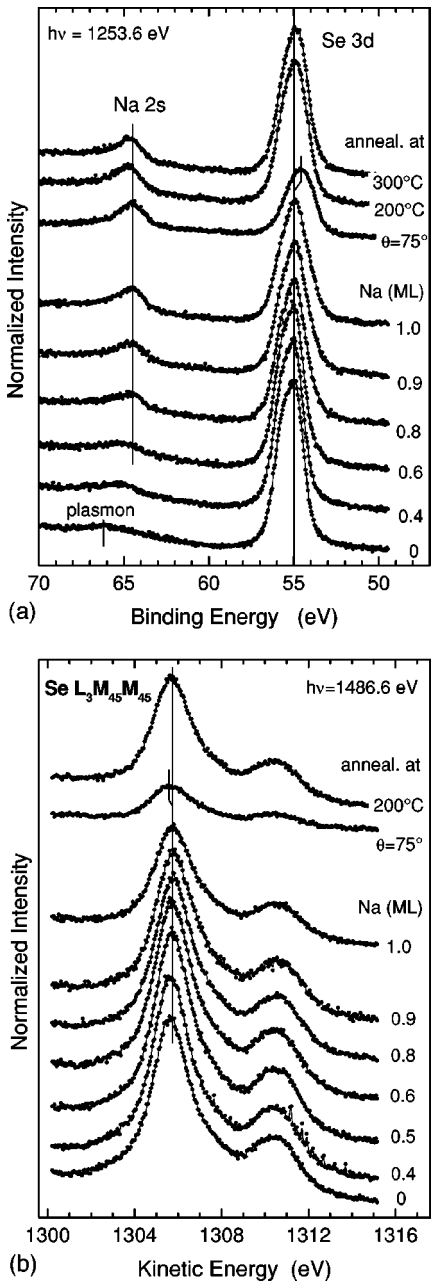

FIG. 5. (a) Mg $K\alpha$-excited Se $3d$ and Na $2s$ spectra of the ZnSe(100)-$c(2\times2)$ surface after stepwise Na deposition at room temperature, and after subsequent annealing. (b) Se $L_3M_{45}M_{45}$ Auger spectra, taken after identical preparation conditions as for (a) (excited by Al $K\alpha$ radiation).

trum recorded at an emission angle of 75°. Due to an insufficient energy resolution, peak fitting to decompose different Se core levels appears to be problematic. Moreover, in Fig. 5(b) no significant line shape change is observed in Se $L_3M_{45}M_{45}$. However, the fact that the Se $3d$ linewidth increases at higher Na coverage indicates that there probably are at least two Se components. This is also confirmed by the following observation: at 1-ML Na coverage the Se $3d$ binding energy of the peak recorded at a normal-emission is higher by 0.4 eV than that recorded at an emission angle of 75°. Also the energy of the Se $L_3M_{45}M_{45}$ Auger transition recorded at normal emission angle is smaller than that taken

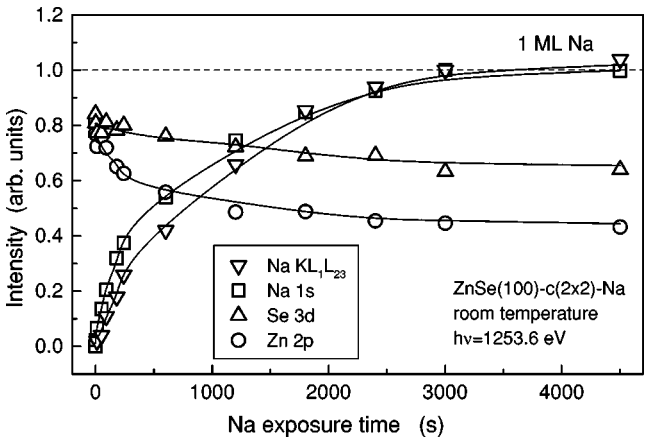

FIG. 6. Relative intensities of Na $1s$, Na KL_1L_{23}, Se $3d$, and Zn $2p_{3/2}$ as a function of Na deposition time at room temperature. The relative intensities of Na $1s$ indicate the Na coverage, as explained in the text. For deposition times larger than ~3000 s, the Na coverage saturates.

at 75°. The existence of at least two Se components implies that the ZnSe-Na interface is now Se terminated (Na-Se bonds).

At higher Na coverage a peak appears at a binding energy of 64.6 eV in Fig. 5(a), which can be attributed to Na $2s$. At 1-ML Na coverage, the intensity ratio of Na $2s$ to Se $3d$ is significantly higher for a larger emission angle (75°) as compared to normal emission (0°). Since for 75° the surface sensitivity is markedly enhanced, this result strongly suggests that the Na atoms do not diffuse into the ZnSe(100) bulk but are located on the ZnSe(100) surface, and that no Se surface segregation occurs at the Na/ZnSe(100) interface at room temperature. These two facts will be further confirmed by a quantitative analysis, described in the following.

Figure 6 shows the relative intensities of the Na $1s$, Na KL_1L_{23}, Se $3d$, and Zn $2p$ peaks plotted vs Na deposition time. The XPS intensities of Zn $2p_{3/2}$ and Se $3d$ decrease with increasing Na coverage, that of Zn $2p_{3/2}$ more rapidly than that of Se $3d$. The different decreases can be accounted for by the different kinetic energies of Zn $2p_{3/2}$ (230 eV) and Se $3d$ (1199 eV) corresponding to different surface sensitivities. Similarly, the Na $1s$ peak should be more surface sensitive than the Na KL_1L_{23} peak, since the kinetic energies are 176 and 950 eV, respectively. However, the intensity evolutions of the Na $1s$ and Na KL_1L_{23} peaks with increasing Na coverage are very similar, corroborating that the Na atoms are indeed located at the surface. The evolution of the Na $1s$ intensity with deposition time explicitly shows a saturation above about 3000 s of Na exposure. Further Na exposure does not result in further Na uptake by the ZnSe(100) surface beyond 1-ML Na coverage. Such saturation effects were also observed for other alkali/semiconductor interfaces.[10] It is well known that the sticking coefficients of alkali atoms on semiconductors such as Si and GaAs decrease at room temperature for coverages close to 1 ML, and become zero beyond 1 ML, due to a much weaker attractive interaction of alkali atoms on alkali adsorbates as compared to that on the interface between substrate and first alkali layer.[10] Of course, the Na saturation behavior on ZnSe(100)-$c(2\times2)$ can also be ascribed to the same physical reason.

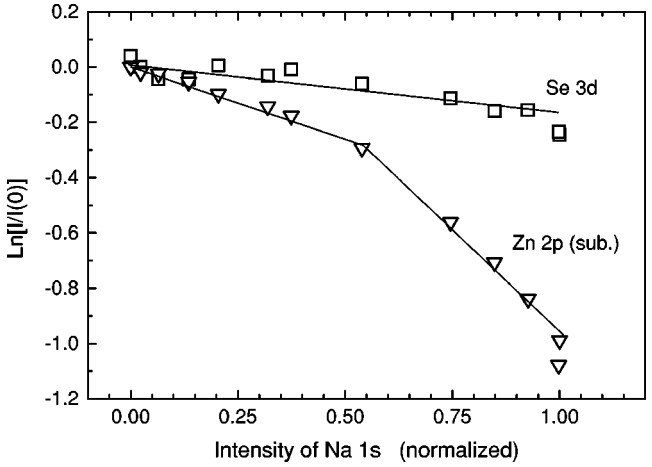

FIG. 7. Attenuation curve of the Zn $2p_{3/2}$ bulk and Se $3d$ components vs Na $1s$ intensity (i.e., Na coverage) indicating two stages of Na adsorption below and above a ''critical'' Na coverage of ~ 0.5 ML.

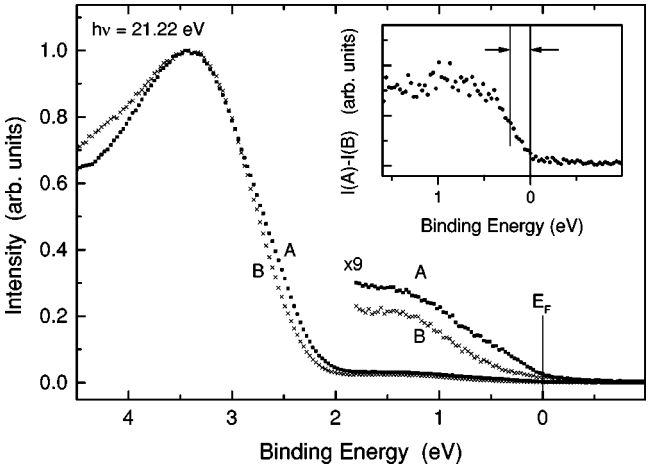

FIG. 8. Valence-band UP spectra of Na/ZnSe(100) interfaces. Curve *A* corresponds to 1 ML Na on ZnSe(100)-$c(2\times2)$. Curve *B* was recorded after annealing at 200 °C. The inset displays a difference curve (*A*-*B*), reflecting a metal-like Fermi level, which is shifted from the Fermi level of the sample holder due to the surface photovoltage effect.

Figure 7 shows the attenuation curves of the Zn $2p_{3/2}$ bulk component and the Se $3d$ peak relative to the Na $1s$ intensity, which corresponds to the Na coverage. The decrease of the Se $3d$ intensity is compatible with a simple attenuation model taking a usual electron inelastic mean free path[18] into account, and assuming that the pristine ZnSe sample becomes covered by 1 ML of Na. The decrease of the Se $3d$ signal is thus incompatible with significant Se segregation at room temperature. The attenuation curve of the Zn $2p_{3/2}$ bulk component clearly shows that the growth of Na on ZnSe consists of two stages: below and above 0.5-ML Na coverage. The initial decrease ($\theta \leqslant 0.5$ ML) of the Zn $2p_{3/2}$ bulk intensity is 2–3 times steeper than that if the Se $3d$ signal, which is consistent with its ~ 2.3 times shorter inelastic mean free path.[18] Therefore, the same argument as used for the Se atoms holds, i.e., the ZnSe sample becomes covered by up to half a monolayer of Na, and no Zn segregation occurs. For $\theta_{Na} \geqslant 0.5$, however, the Zn $2p_{3/2}$ bulk signal drops drastically, which can only be explained if Zn atoms disappear from the interface region, such that they no longer contribute to the Zn bulk signal. This is in perfect agreement with the appearance of a ''metallic'' Zn species (the signal of which has not been included in Fig. 7). Since the intensity of this Zn species is relatively high for $\theta_{Na}=1$ (see Figs. 2 and 3) and markedly increases at grazing emission angle (see Fig. 3) we infer that it stems from an exchange reaction with Na and from segregation and island formation on top of the Na layer.

This conclusion is corroborated by the following annealing experiment. It can be expected that the metallic Zn species can be desorbed upon annealing in UHV, since the Zn vapor pressure is relatively high (of the order of 10^5 mbar at 200 °C). Figure 3 (top spectra) shows indeed that the metallic Zn component (the kinetic energy is 1014.6 eV) disappears upon annealing at 200 °C for 5 min. In addition, Fig. 4 shows that the Na $1s$ intensity remains approximately unchanged upon this annealing step and that the Auger parameter of the Na species also remains nearly constant, i.e., nonmetallic. The Na intensity slightly decreases upon further annealing at 300°C for 5 minutes. This clearly confirms the above conclusion that there is no metallic Na on the surface, since the vapor pressure of metallic Na is of the order of 10^{-4} mbar at 200°C. At the same time, the line shapes of Se $3d$ and Se $L_3M_{45}M_{45}$ remain nearly unchanged upon annealing at 200 °C, as shown in Fig. 5. This implies that the Se-Na and Se-Zn bonds have similar chemical characters.

The question about the metallization of the surface by the metallic Zn species still remains to be discussed. Figure 8 shows the valence-band UV photoelectron spectra excited with He I radiation ($h\nu = 21.22$ eV). Curve *A* corresponds to the spectrum of ZnSe(100)-$c(2\times2)$ with 1-ML Na coverage. Curve *B* was recorded after this interface was annealed at 200 °C. The enlarged part of curve *B* clearly shows a structure around 1.5 eV which is mainly due to a He I satellite contributions from the peak at 3.4 eV. This similar structure of curve *A* is contributed from both the He I satellite intensity and the ''metallic'' Zn species. This is consistent with the observation that after annealing at 200 °C the ''metallic'' Zn species disappears, while the Na intensity nearly stays constant, and the Na species remains nonmetallic. Hence the difference between curves *A* and *B* mainly originates from the ''metallic'' Zn species. As shown in the inset of Fig. 8, the difference spectrum clearly shows a metallic ''cutoff,'' i.e., a Fermi level. This Fermi level deviates from the Fermi level of the sample holder by ~ 0.2 eV which is due to a surface photovoltage effect,[18] widely observed in photoemission spectra of ZnSe(100) surfaces.[1,15] The appearance of a Fermi level indicates that the ''new'' Zn species becomes metallic when approaching the Na saturation coverage due to the proposed cation exchange reaction between Na and Zn atoms which most probably leads to the formation of metallic Zn islands on the topmost layer. This implies that the Se-Na bond is energetically more favorable (and hence stronger) than the Se-Zn bond. It may be further inferred that Na can be doped in ZnSe to an appreciable extent, although not all Na doping atoms may be electrically active. Finally, the possibility that Na atoms are located at interstitial sites cannot account for the appearance of a metallic Zn species

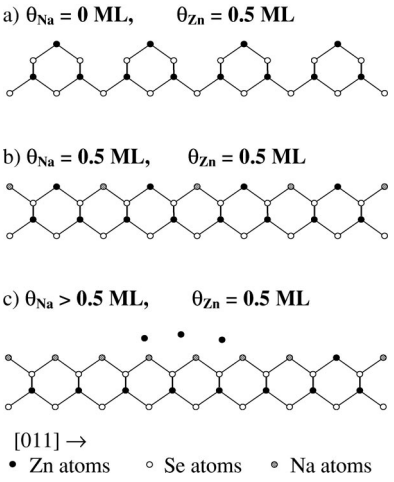

FIG. 9. Simplified Na/ZnSe(100)-$c(2\times2)$ interface model for (a) the clean ZnSe(100)-$c(2\times2)$ surface, (b) 0.5 ML of Na on ZnSe(100), and (c) 1 ML of Na on ZnSe(100). In the last case a cation exchange reaction occurs between Na and the topmost Zn atoms, which leads to the formation of metallic Zn islands on top of the surface.

because in this case no exchange reaction would occur. Hence the limited hole concentration in Na-doped ZnSe is due neither to the compensation of interstitial Na donor atoms nor to a lack of Na dissolution in ZnSe.

B. Structural model of Na/ZnSe(100) interfaces

On the basis of the above analysis, we propose a simplified interface model for the ZnSe(100)-$c(2\times2)$-Na interfaces prepared at room temperature, as shown in Fig. 9. From photoemission,[13,15] atomic-layer epitaxy,[19] and first-principles total-energy calculations,[20,21] it can be concluded that the sputter-annealed ZnSe(100)-$c(2\times2)$ surface is Zn terminated with 0.5-ML Zn coverage, as depicted in Fig. 9(a). The ZnSe(100)-$c(2\times2)$-Na interface formation is composed of two stages, below and above a critical Na coverage ($\sim$0.5 ML). In the first stage, as shown in Fig. 9(b), the Na atoms chemisorb on top of the ZnSe(100) surface in empty Zn sites. In the second stage, while further increasing the Na coverage, Na atoms replace top Zn atoms, as shown in Fig. 9(c). The corresponding Zn atoms segregate on top of the Na layer and eventually form metallic Zn islands at the Na saturation coverage. In other words, the cation exchange reaction between Na and Zn atoms occurs above a critical Na coverage of 0.5 ML. Due to the clustering of Zn atoms, a part of the Na overlayer remains uncovered, while the rest is covered by metallic Zn islands. A cation exchange reaction was also observed for metal/III-V semiconductor interfaces, such as Al/GaAs and Al/GaP.[22,23]

This interface model can well account for all above-mentioned experimental observations. For example, the partly covered and partly uncovered Na layer by metallic Zn can account for the various chemical species of Na, since metallic Zn islands on top lead to different initial- and final-state effects for the covered Na atoms as compared to the uncovered Na atoms. In addition, this model also explains the unusual relative Zn $L_2M_{45}M_{45}$ intensities, as shown in Fig. 3(b). The metallic Zn component originates from the topmost Zn layer ontop of the Na-covered ZnSe(100) surface. Thus it seems to be impossible, at first glance, that this Zn component shows an Auger intensity comparable to that of the Zn bulk component, since the kinetic energy of Zn $L_2M_{45}M_{45}$ is approximately 1010 eV, and thus not very surface sensitive. However, as the metallic Zn islands and the next Zn layer of the ZnSe substrate are separated by one Na layer and then by one Se layer, the attenuation of the next (bulk) Zn layer is significant, and hence the metallic Zn $L_2M_{45}M_{45}$ Auger peaks show a relatively large intensity.

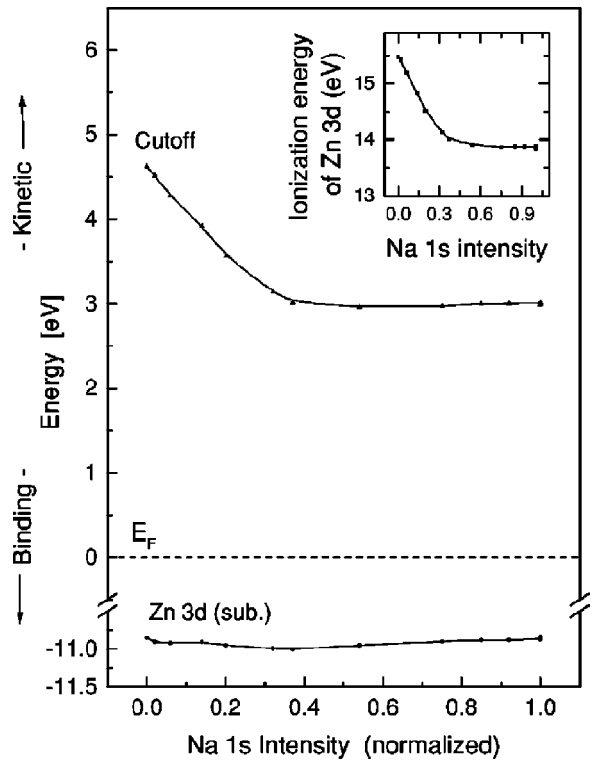

FIG. 10. Energy shift of the Zn 3d shallow core level and of secondary electron cutoff (corresponding to the vacuum level), as a function of Na coverage. The inset shows the evolution of the Zn 3d ionization energy with increasing Na coverage.

C. Band bending, surface dipole, and Fermi-level pinning

Figure 10 shows the evolution of the Zn 3d substrate component and of the secondary electron cutoff with increasing Na coverage on binding- and kinetic-energy scales, respectively. The cutoff corresponds to the vacuum level of the surface. The Zn 3d binding energy reflects the band bending of Na/ZnSe(100) interfaces under UV irradiation. Band bending generally arises from various effects including (1) intrinsic surface states stemming from the discontinuity of the lattice potential and bonding at the vacuum-solid interface;[24] (2) extrinsic surface states due to lattice imperfections; (3) extrinsic interface states due to local lattice deformation and localized atomic bonding involving, e.g., Na atoms; (4) metal-induced gap states[25] due to wave-function tunneling from the metallic islands into the substrate band gap; and (5) surface photovoltage effects.[18] However, with the above-mentioned experimental results, it appears to be difficult to separate these effects in the present case.

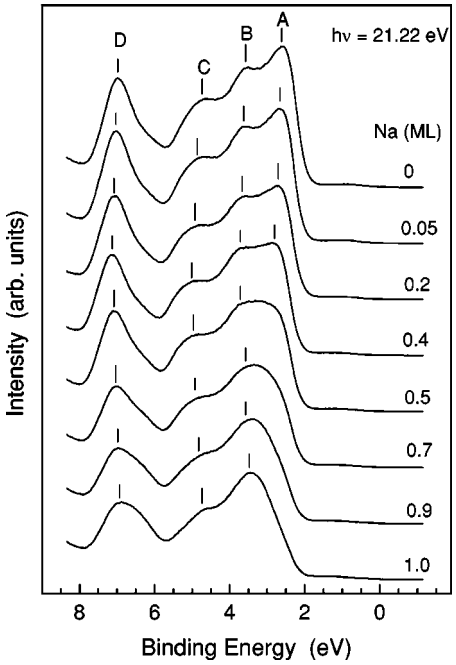

FIG. 11. (Partly) angle-resolved valence-band UP spectra taken for different Na coverages at normal emission.

The secondary electron cutoff reflects the work function of the Na/ZnSe(100) interface (under UV irradiation). Band bending and the surface dipole determine the work function. The energy difference between the (negative) binding energy of the Zn $3d$ and the secondary electron cutoff is the so-called ionization energy of Zn $3d$, as shown in the inset of Fig. 10. Since the Zn $3d$ bulk component reflects the band bending, the Zn $3d$ ionization energy just indicates the evolution of the surface dipole, which drops rapidly with increasing Na coverage up to ~ 0.4 ML. The surface dipole can be decreased by 1.7 eV due to the rather electropositive Na. Such a drastic change of the surface dipole is expected to reduce the metal/p-ZnSe Schottky barrier significantly. However, our recent investigations of Au/ZnSe(100) and Au/Na/ZnSe(100) interfaces using photoemission show a Fermi-level pinning behavior of the Schottky barrier for Na interface doping.[15] Based on these preliminary results, which show a reduction of the barrier by 0.16 eV, it is most probable that the metallic Zn islands and/or interdiffusion of Na and Au atoms prevent a more significant reduction of the ZnSe Schottky barrier. We may argue that an improved contact to p-ZnSe could be realized in a metal/alkali/p-ZnSe(100) system, in which alkali atoms can be incorporated as the δ layer, and for which the metal/p-ZnSe interface is abrupt.

D. Valence-band states and surface states

UPS was used to characterize the evolution of the occupied valence-band states during the formation of the Na/ZnSe(100)-$c(2\times2)$ interface. While a full analysis of the surface electronic states requires measurements with high angular resolution and variation of angle and/or photon energy, the spectra presented in Fig. 11 are taken with poor angular resolution ($\pm 8°$). These spectra indicate changes in the valence band associated with the Na coverage. For the clean ZnSe(100)-$c(2\times2)$ surface, peaks labeled *A*, *B*, *C*, and *D* are noted at binding energies of 2.6, 3.6, 4.7, and 7.0 eV; the linearly extrapolated valence-band maximum has a binding energy of 2.0 eV (the small shoulder at a binding energy of ≈ 1 eV is due to the above-mentioned He I satellite. Thus peaks *A*, *B*, *C*, and *D* are located at 0.6, 1.6, 2.7, and 5.0 eV relative to the valence-band maximum. These peaks agree well with previous XPS and UPS results from this surface.[26,27] With increasing Na coverage, peak *A* becomes weaker and finally disappears. Simultaneously, the energy positions of peaks *B*, *C*, and *D* change, while their relative energy distances remain nearly constant. The energy shift of the three peaks is consistent with the observed band bending, as shown in Fig. 10. This indicates that peaks *B*, *C*, and *D* originate from bulk states[26] or so-called surface-induced bulk states, which arise from the boundary condition introduced by the surface.[28] For ZnSe(100), such states are predicted to occur at 2.0, 2.3, and 5.3 eV relative to the valence-band maximum,[28] independent of the surface termination. Thus, they may also be associated with the observed peaks *B*–*D*. In addition, since peak *A* disappears upon Na exposure, it can be identified as a surface state, as predicted by first-principles total-energy calculations.[21] According to these calculations, one surface state lies below the valence-band maximum and arises from the dangling-bond states of the Se atoms, but unfortunately, no accurate energy position has been given.[21] However, due to its disappearance upon alkali deposition we can identify peak *A* in Fig. 11 as this surface state in the present study.

IV. SUMMARY

We have studied the initial phase of the ZnSe(100)-$c(2\times2)$-Na interface formation using LEED, XPS, UPS, and XAES. Na has been deposited on a $c(2\times2)$-reconstructed ZnSe(100) surface at room temperature up to a coverage of ~ 1 ML. In this coverage regime, the growth of Na on the ZnSe(100)-$c(2\times2)$ surface can be divided into two stages: below and above ~ 0.5-ML Na coverage. Below 0.5-ML coverage, Na atoms are adsorbed on empty Zn sites available on a Zn-terminated ZnSe(100) surface which has about half a monolayer of Zn coverage. Above 0.5-ML Na coverage the ZnSe(100)-Na interface becomes reactive and a cation exchange reaction occurs between Na atoms and the top Zn atoms of the formerly Zn-terminated surface. The exchanged Zn atoms segregate on top of the Na overlayer, eventually forming metallic Zn islands. The surface dipole of ZnSe(100)-$c(2\times2)$ can be decreased by 1.7 eV by Na exposure. In addition, Na deposition allows the identification of a surface state 0.6 eV below the valence-band maximum. However, it still remains to be demonstrated whether Ohmic contacts to p-ZnSe can be realized by alkali interface doping.

ACKNOWLEDGMENTS

We thank Dr. Clemens Heske for a critical reading of the manuscript. This work was supported by the Deutsche Forschungsgemeinschaft within SFB410. One of us (Z.H.C.) would like to thank the Volkswagen-Stiftung for financial support.

*On leave from National Laboratory of Infrared Physics, Shanghai Institute of Technical Physics, Chinese Academia Sinica, Shanghai, 200083, China.

[1] W. Chen, A. Kahn, P. Soukiassian, P.S. Mangat, J. Gaines, C. Ponzoni, and D. Olego, Phys. Rev. B **51**, 14 265 (1995).

[2] M. Vos, Steven G. Anderson, and J.H. Weaver, Phys. Rev. B **39**, 3274 (1989).

[3] M. Vos, F. Xu, Steven G. Anderson, J.H. Weaver, and H. Cheng, Phys. Rev. B **39**, 10 744 (1989).

[4] P. Soukiassian, M.H. Bakshi, H.I. Starnberg, Z. Hurych, T.M. Gentle, and K.P. Schuette, Phys. Rev. Lett. **59**, 1488 (1987).

[5] P. Soukiassian, M.H. Bakshi, Z. Hurych, and T.M. Gentle, Phys. Rev. B **35**, 4176 (1987).

[6] P. Perfetti, C. Quaresima, C. Coluzza, C. Fortunato, and G. Margaritondo, Phys. Rev. Lett. **57**, 2065 (1986).

[7] M.A. Haase, J. Qiu, J.M. DePuydt, and H. Cheng, in *Proceedings of the 18th International Symposium on Gallium Arsenide and Related Compounds, Seattle, Washington, 1991*, edited by G. B. Stringfellow (Institute of Physics Publishing Ltd., Bristol, 1991), p. 9.

[8] *NBS Tables of Chemical Thermodynamic Properties,* [J. Phys. Chem. Ref. Data Suppl. **11**, 2 (1982)].

[9] D. Mao, M. Santos, M. Shayegan, A. Kahn, G. Le Lay, Y. Hwu, G. Margaritondo, L.T. Florez, and J.P. Harbison, Phys. Rev. B **45**, 1273 (1992).

[10] See, e.g., C.A. Sébenne, in *Handbook on Semiconductors*, edited by T.S. Moss and M. Balkanski (Elsevier, Amsterdam, 1994), Vol. 2, Chap. 2, p. 35, and references therein.

[11] W. Weiss, Ph.D. thesis, Universität Stuttgart, 1993.

[12] J.J. Joyce, M. Del Giudice, and J.H. Weaver, J. Electron Spectrosc. Relat. Phenom. **49**, 31 (1989).

[13] W. Chen, A. Kahn, P. Soukiassian, P.S. Mangat, J. Gaines, C. Ponzoni, and D. Olego, Phys. Rev. B **49**, 10 790 (1994).

[14] F. Xu, M. Vos, J.H. Weaver, and H. Cheng, Phys. Rev. B **38**, 13 418 (1988).

[15] Z. Chen, D. Eich, R. Fink, and E. Umbach (unpublished).

[16] D. Briggs and M.P. Seah, in *Practical Surface Analysis*, 2nd ed. (Wiley, Chichester, 1990), p. 595.

[17] M. Alonso, R. Cimino, and K. Horn, Phys. Rev. Lett. **64**, 1947 (1990).

[18] M.P. Seah and W.A. Dench, Surf. Interface Anal. **1**, 2 (1979).

[19] See, e.g., J. Lilja, J. Keskinen, M. Hovinen, and M. Pessa, J. Vac. Sci. Technol. B **7**, 593 (1989).

[20] A. Garcia and J.E. Northrup, Appl. Phys. Lett. **65**, 708 (1994).

[21] C.H. Park and D.J. Chadi, Phys. Rev. B **49**, 16 467 (1994).

[22] C.B. Duke, A. Paton, R.J. Meyer, L.J. Brillson, A. Kahn, D. Kanani, J. Carelli, J.L. Yeh, G. Margaritondo, and A.D. Katnani, Phys. Rev. Lett. **46**, 440 (1981).

[23] A.B. McLean, I.T. McGovern, C. Stephens, W.G. Wilke, H. Haak, K. Horn, and W. Braun, Phys. Rev. B **38**, 6330 (1988).

[24] J. Bardeen, Phys. Rev. **71**, 717 (1947).

[25] S.G. Louie and M.L. Cohen, Phys. Rev. B **13**, 2461 (1976).

[26] J.R. Chelikowsky, T.J. Wagener, J.H. Weaver, and A. Jin, Phys. Rev. B **40**, 9644 (1989).

[27] G.P. Lopinski, J.R. Fox, J.S. Lannin, F.S. Flack, and N. Samarth, Surf. Sci. **355**, L355 (1996).

[28] D. Olguin and R. Baquero, Phys. Rev. B **51**, 16 891 (1995).